DOI: 10.61782/fa.2025.0832

FORUM ACUSTICUM
EURONOISE 2025

STREAMLINED MODEL OF POROUS MEDIA FOR FINITE DIFFERENCE TIME DOMAIN SCHEMES

P.C. Iglesias[1*] **L. Godinho**[2] **J. Redondo**[1]

[1] Instituto de Investigación para la Gestión Integrada de Zonas Costeras, Universitat Politècnica de València, Spain

[2] Departamento de Engenharia Civil, Universidade de Coimbra, ISISE, ARISE, Portugal

ABSTRACT

Extracting the microscopic parameters of a porous material is a challenging task, and efforts have been made to create models that simulate their properties with minimal data. For example, tests to assess macroscopic behaviors like tortuosity, which is directly related to microscopic behavior, can lead to errors if the measurement tools are not accurate, and the same applies to other parameters. Therefore, we have developed a minimalistic sound propagation model in porous materials with a rigid frame, based on local theory, aimed at simplifying the process of obtaining the fundamental macroscopic characteristics of porous materials, such as their absorption coefficient at normal and random incidences, as well as their normal surface impedance. The proposed linearized equivalent-fluid model includes four phenomenological coefficients that describe acoustic propagation through the material. These coefficients are determined by the material's thickness and with impedance tube absorption measurements following the ISO 10534 standard. Consequently, only the measured absorption coefficient—either in one-third or one-octave bands—is needed to fully characterize the material acoustic behavior. The model has been simulated using the Finite Difference Time Domain scheme, and the results show strong agreement with the laboratory measurements and other well-established semi-phenomenological models.

Keywords: *porous absorber, FDTD, equivalent porous material.*

[*] ***Corresponding author***: *pabcamig@gmail.com*

1. INTRODUCTION

Sound propagation within the pores of porous absorbers is often characterized by its effective density, excluding thermal effects, and its effective bulk modulus, disregarding viscous effects [1]. Under harmonic conditions, the material can be represented macroscopically as an equivalent fluid governed by local equations [2]. The initial theoretical formulations were introduced by Johnson [3] and later refined by Lafarge, leading to the widely adopted JCAL (Johnson-Champoux-Allard-Lafarge) model [4], which is commonly used to estimate sound absorption in porous materials. The literature offers a limited number of porous material models applicable to FDTD. While some analytical time-domain models exist for rigid-frame porous materials, their high computational demands hinder practical implementation. In this paper, the Numerical Equivalent Acoustic Material (NEAM) is proposed, a model with equivalent properties that enable accurate time-domain simulations of material behavior. The NEAM model replaces low-frequency parameters with phenomenological coefficients, which must be adjusted to ensure that the simulated absorption coefficients match those obtained from Kundt tube measurements.

2. MATERIALS & METHODS

2.1 Neam Model

Sound propagation within a porous material can be described in time domain using the equations given at the JCAL model [4]. In the frequency domain, using the exponential notation, these equations can be then transformed into:

$$i\omega\rho_{ef}\bar{V}_m = -\nabla\bar{p}_m \quad (1)$$

$$i\omega C_{ef}\bar{p}_m = -\nabla\cdot\bar{V}_m \quad (2)$$

where ρ_{ef} is the effective density, C_{ef} is the effective compressibility, V_m and P_m are the frequency-dependent particle velocity and pressure, respectively.

Following Alomar et al. [5], partial fraction expansion of the effective density and compressibility leads to the forms:

$$\rho_{ef}(\omega) \approx \rho_\infty + \sum_{k=1}^{Np} \frac{A}{i\omega + a_k} \tag{3}$$

$$C_{ef}(\omega) \approx C_\infty + \sum_{k=1}^{Nc} \frac{B}{i\omega + b_k} \tag{4}$$

Where ρ_∞ and C_∞ are the asymptotic values of density and compressibility as frequency tends to infinity, A and B are real constants, and a_k and b_k are the poles of the functions. As noted by Moufid et al. [6], the poles must be positive to ensure stable solutions.

Substituting Equations (3) and (4) into Equations (1) and (2), along with the auxiliary functions φ_m and ϕ_m related to the convolution integrals of particle velocity and pressure, the inverse Fourier Transform gives:

$$\rho_\infty \frac{\partial u_m}{\partial t} + \sum_{k=1}^{Np} A u_m - \sum_{k=1}^{Np} A a_k \varphi_m = -\nabla p_m \tag{5}$$

$$\frac{1}{\rho_\infty c_\infty^2} \frac{\partial p_m}{\partial t} + \sum_{k=1}^{Nc} B p_m - \sum_{k=1}^{Nc} B b_k \phi_m = -\nabla \cdot u_m \tag{6}$$

As in example, φ_m along X-axis gives the next convolution term:

$$\varphi_m(x,t) = \int_0^t u_m(x,t') e^{-a_k(t-t')} dt' \tag{7}$$

The convolution terms in Equations (5-6) reflect the material's non-instantaneous response, accounting for dispersion effects. If the material is assumed to have an immediate action-response behavior, the integral contribution can be neglected, simplifying Equations (5-6) to:

$$\rho_\infty \frac{\partial u_m}{\partial t} + \sum_{k=1}^{Np} A u_m = -\nabla p_m \tag{8}$$

$$\frac{1}{\rho_\infty c_\infty^2} \frac{\partial p_m}{\partial t} + \sum_{k=1}^{Nc} B p_m = -\nabla \cdot u_m \tag{9}$$

In both cases, the discrete summation in Equations (8-9) should yield a numerical real value, and can thus be replaced by a constant, frequency-independent variable. Similarly, the asymptotic values of density and compressibility can be replaced by real values, leading to the introduction of the concepts of equivalent effective density Ω and equivalent effective compressibility Ψ, as in the JCAL model.

The proposed Numerical Equivalent Acoustic Material (NEAM) describes porous materials using real values for numerical tortuosity, Ω_A, and numerical viscosity, Ω_B, which account for viscous and inertial interactions, while the density remains solely dependent on the propagation medium. Given that thermal exchanges between the fluid and structure may occur due to frame elasticity — leading to compression-expansion variations — additional variables are needed to capture this behavior. Consequently, numerical compressibility, Ψ_A, and numerical thermolability, Ψ_B, are introduced. Similarly, static compressibility is considered dependent only on the propagation medium.

Just as the equivalent tortuosity and viscosity remain independent of frequency, the equivalent compressibility and thermolability do as well. As demonstrated in later sections, omitting the convolution term still yields acceptable results, suggesting that characterizing porous materials without this term could significantly expand the applicability of time-domain methods. The NEAM model is therefore defined as follows:

$$\Omega_A \frac{\partial u_m}{\partial t} + \Omega_B u_m = -\rho_0^{-1} \nabla p_m \tag{10}$$

$$\Psi_A \frac{\partial p_m}{\partial t} + \Psi_B p_m = -\rho_0 c^2 \nabla u_m \tag{11}$$

For $\Omega_A \neq \Omega_B \neq \Psi_A \neq 0$, and $\Psi_B = 0$, the NEAM model approximates the low-frequency model. Furthermore, when $\Omega_A = \Psi_A = 1$ and $\Omega_B = \Psi_B = 0$, the NEAM formulation converges to the linearized lossless governing equations (momentum and mass conservation).

2.2 Neam coefficients

To determine appropriate values for the NEAM model coefficients (Ω_A, Ψ_A, Ω_B, Ψ_B), input data from a given material is required. Specifically, only the sound absorption coefficient—measured at normal incidence—and the material thickness are needed for the calculation. The simplicity of the proposed NEAM method makes it an attractive option for practical applications.
An iterative optimization algorithm is used to compare the simulated absorption coefficient with the measured value, adjusting the equivalent parameters accordingly. Since these coefficients must accurately represent a complex physical phenomenon, their evaluation is constrained to

ensure a single, well-defined solution, as illustrated in Figure 1.

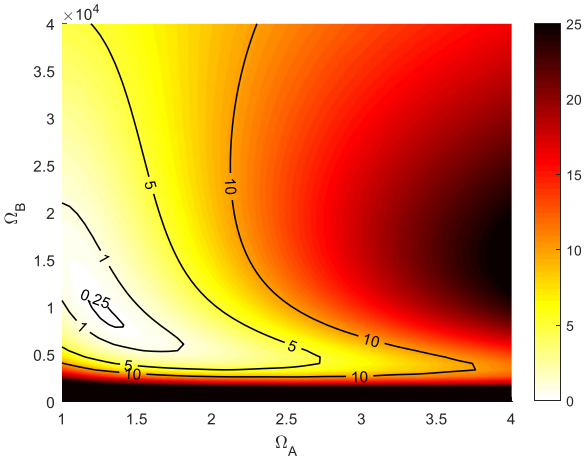

Figure 1. Computed space exploration for 1D simulation with a melamine foam porous absorber of 60 mm thickness. Figure shows the quadratic error, in percentage, with respect to an input data measured in an impedance tube with ISO 10534-2.

2.3 FDTD Method

Domain constitutive equations can characterize a linear fluid without losses and are formulated using Euler's continuity equation and the momentum equation [7]. The solution of equations (10-11) can be achieved through the classical FDTD method, where the partial derivatives in the constitutive equations are approximated using central finite difference schemes. These schemes employ staggered grids for both pressure and particle velocity vector in space and time [8]. Given the finite dimensions of the simulation domain, the computational space must be constrained to prevent unwanted reflections from interfering with the region of interest. To mitigate such spurious reflections, a perfectly matched layer (PML) is applied, following the approach referenced in [8].

For normal and oblique wave incidence, 1D and 2D FDTD schemes were implemented, respectively. Simulations were carried out using 20 points per wavelength PPWL, considering an upper frequency of $4k\sqrt{2}$. In the NEAM modeling algorithm, the first step involves normal incidence evaluation. The objective is twofold: first, to compare the simulated absorption coefficients with impedance tube measurements as per ISO 10534, parts I and II; and second, to determine the equivalent coefficients for use in 2D FDTD simulations (oblique incidence). A quadratic PML was applied on one side of the FDTD domain, while a NEAM with an impervious wall at the rear was placed on the opposite side. The algorithm employs a summed multiple Ricker wavelet as the input signal, designed to achieve a flat frequency response across the 125 Hz to 4 kHz octave bands. Incident and reflected wave components were then extracted using a suitable time-windowing technique. The complex reflection coefficient, R, was subsequently determined via transfer function as,

$$R = FFT\{p_R\} / FFT\{p_I\} \tag{12}$$

where FFT represents the Fast Fourier Transform, p_R reflected pressure and p_I incident pressure. From this, the normal incidence absorption coefficient was computed as in [7],

$$\alpha_n = 1 - |R|^2 \tag{13}$$

A similar methodology was employed in the 2D FDTD framework. In this case, oblique incidence was analyzed through individually angled simulations, enabling the determination of random incidence sound absorption using Paris' integration [9]. The use of oblique incidence in the 2D FDTD approach was considered to assess whether the 1D virtual coefficients (from normal incidence) could also account for diffuse sound behavior. To control the signal incidence angle, periodic boundary conditions were implemented at the top and bottom of the 2D domain, using the sine-cosine method described in [8]. Since the 2D model exhibits periodicity in the Y direction, the NEAM effectively behaves as an infinitely extended material. Consequently, the absorption coefficient results should not be compared with ISO 354 measurements, which are based on finite-size samples. Instead, analytical calculations for infinite samples must be employed. Due to the frequency-dependent nature of periodic boundaries, the Ricker wavelet is no longer utilized. Instead, sinusoidal waves at one-third octave bands from 100 Hz to 5 kHz are used. The absorption coefficient is then determined using the standing wave method outlined in ISO 10534-1.

3. RESULTS

This section provides the results summary obtained from FDTD simulations. The NEAM model has been calibrated for various materials, demonstrating its versatility across different kernels. While originally designed to simulate the macroscopic behavior of porous absorbers, its adaptability allows it to be applied to other material types, such as fiber-based structures. To illustrate this, simulations were

conducted on two different materials: melamine foam (a porous absorber) and a PET sheet (a fiber material). Their results were then compared with experimental measurements and analytical calculations. Section 3.1 presents the findings for melamine foam, Section 3.2 covers the PET sheet results, and Section 3.3 evaluates the overall performance of the algorithm.

3.1 Melamine foam results

In reference [10], absorption results for a 60 mm material sheet are provided and are used here as a benchmark for comparison with the NEAM model. Figure 2 illustrates the normal incidence absorption coefficient obtained through the 1D FDTD simulations, showing a strong resemblance to the measured data. However, below 315 Hz, the model slightly overestimates absorption, with a maximum deviation of 0.06 at 125 Hz. This discrepancy could stem from potential errors in normal incidence measurements at low frequencies due to tube length limitations. Notably, reference [10] does not provide details on the experimental setup, to the best of the authors' knowledge.

Additionally, a mismatch is observed at 4 kHz and 5 kHz, likely caused by the one-third octave band averaging applied to the continuous FDTD data. This averaging process smooth out fluctuations, causing certain values to be lost and resulting in a flattened absorption response between 3150 Hz and 5000 Hz, which is not present in the original FDTD calculations. Figure 3 displays the normal incidence surface impedance, which aligns well with the analytical results obtained using the JCAL model. However, above 2 kHz, slight deviations from the 2D FDTD results can be noted. These discrepancies may be attributed to two factors: (a) the mismatch in normal incidence absorption at the 2 kHz band in Figure 4, which increases absorption and, consequently, impedance; and (b) dispersion effects in the FDTD method that may shift peak frequencies.

At low frequencies, the material behaves as a purely reactive and capacitive system, similar to an open electrical circuit, where voltage (analogous to pressure) is at its maximum and no pressure drop occurs across the material. Figure 4 presents the diffuse sound absorption, showing a strong correlation with analytical data. As with the 1D FDTD results, a minor deviation is observed at higher frequencies, though the overall error remains negligible. At lower frequencies, the comparison remains consistent, but unlike the 1D model, the 2D approach accounts for multiple angles of incidence, leading to a more uniformly smoothed absorption coefficient response.

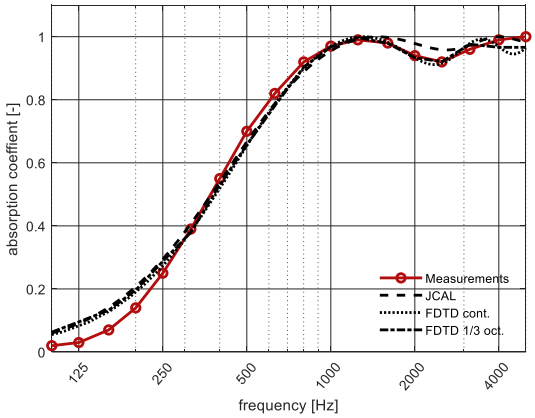

Figure 2. 60 mm melamine foam normal incidence sound absorption computed with 1D-FDTD scheme compared with ISO 10534 measurements (red line), black line is the FDTD full calculation, and blue line is the black line averaged to 1/3 octave bands.

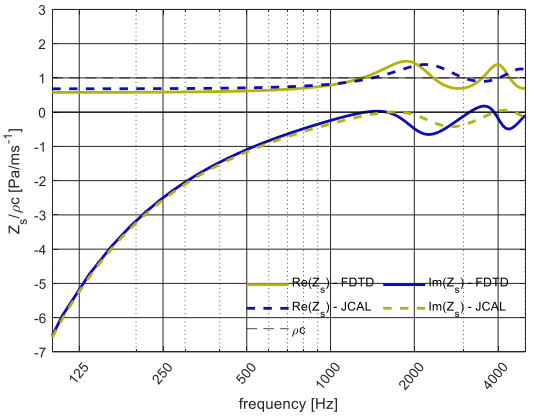

Figure 3. 60 mm melamine foam surface impedance at normal incidence computed with 1D-FDTD scheme.

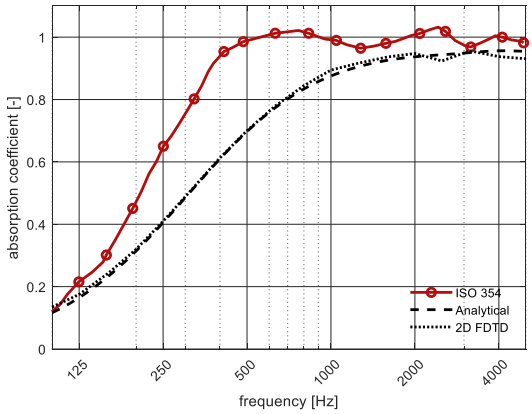

Figure 4. 60 mm melamine foam diffuse field calculated using oblique incidence absorption and Paris' formulation.

3.2 PET sheet results

In reference [11], a series of PET fiber sheets were tested to differentiate between pure and recycled PET. These materials typically exhibit moderate absorption, primarily at high frequencies. This study focuses on comparing the normal incidence sound absorption of a 40 mm recycled PET sheet with a surface density of 1.2 kg/m². Since reference [11] does not provide macroscopic parameters for the JCAL model, a reverse engineering approach was used to derive the five necessary parameters from the absorption coefficient data.

Figure 5 demonstrates strong agreement between the 1D FDTD simulation results and experimental measurements. However, the reverse JCAL model shows some variation at low frequencies (below 315 Hz), leading to lower calculated absorption in that range. Figure 6 presents the normal incidence surface impedance, revealing a capacitive behavior at low frequencies, similar to that of a porous absorber. However, below 250 Hz, the real part of the impedance increases in the 2D FDTD results, which correlates with an increase in material absorption. At higher frequencies, a slight deviation at the peak frequency may be attributed to dispersion effects in the FDTD method. Nevertheless, the comparison between the NEAM model results and analytical data remains highly accurate.

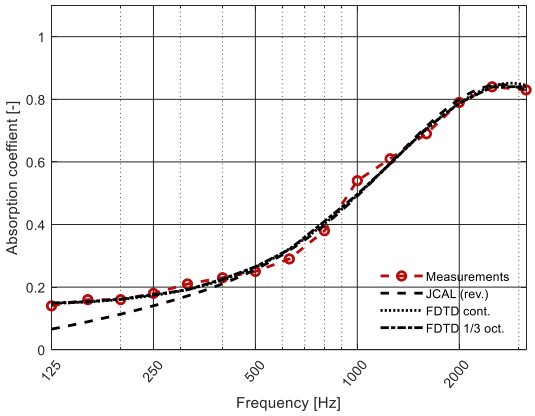

Figure 5. 40 mm PET sheet normal incidence sound absorption computed with 1D-FDTD scheme compared with ISO 10534 measurements (red line), black line is the FDTD full calculation, and blue line is the black line averaged to 1/3 octave bands.

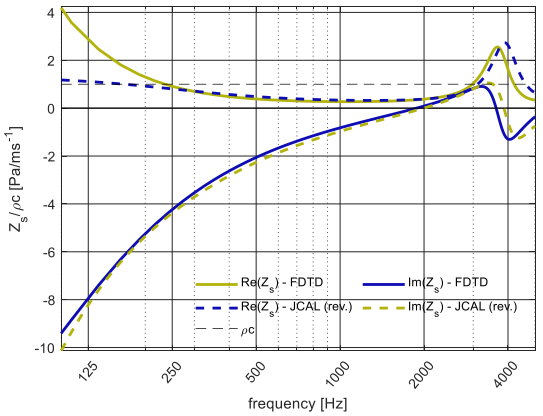

Figure 6. 40 mm PET surface impedance at normal incidence computed with 1D-FDTD scheme.

Lastly, Figure 7 illustrates the diffuse sound absorption, showing excellent alignment with theoretical predictions. Below 315 Hz, however, the simulated absorption exceeds the analytical results. Given that the JCAL model is specifically designed for porous absorbers, it is uncertain whether this discrepancy indicates an actual issue. Theoretical 1D calculations suggest that at low frequencies, the NEAM model aligns well with impedance tube measurements, whereas the JCAL model tends to underestimate absorption. Since the same parameters were used for diffuse field calculations, any initial error in parameter estimation may have propagated into the results, leading to differences between the FDTD and analytical outcomes.

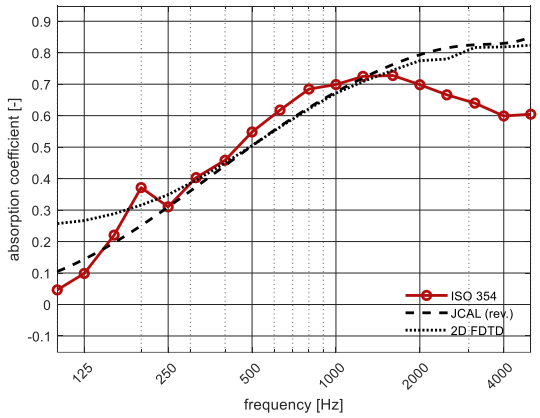

Figure 7. 40 mm PET diffuse field calculated using oblique incidence absorption and Paris formulation.

3.3 Algorithm performance

The complete performance analysis is provided exclusively for the 60 mm melamine foam sheet. Due to the exponential increase in computation time at low frequencies, as discussed in a later section, performance evaluations for 2D FDTD simulations were conducted within the 315 Hz to 5 kHz range.

Section 3.3.1 examines the NEAM model's behavior under different PPWL values, which can help to optimize computational efficiency. Section 3.3.2 investigates the minimum simulation time required to accurately capture the pressure inside the tube for each frequency and incidence angle, along with defining a stopping criterion for the algorithm. Lastly, Section 3.3.3 outlines the computational costs using a six-core AMD Ryzen 5 4500U processor running at 3.40 GHz with 32 GB of DDR4 RAM.

3.3.1 PPWL analysis

This study analyzes absorption coefficient results using different PPWL configurations for both 1D and 2D schemes. Figure 8 compares various PPWL values in the 1D FDTD scheme with measurements taken in a Kundt tube. As shown in the figure, no significant differences are observed. Consequently, for the 1D case, even the lowest value of 6 PPWL produces accurate results.

Since the NEAM model adapts to the given input data while maintaining a fixed set of FDTD parameters, the absorption coefficient results in the 1D FDTD scheme remain consistent, with variations occurring only in the NEAM coefficient values. In reality, noticeable differences arise only when combining different PPWL values between the 1D and 2D schemes.

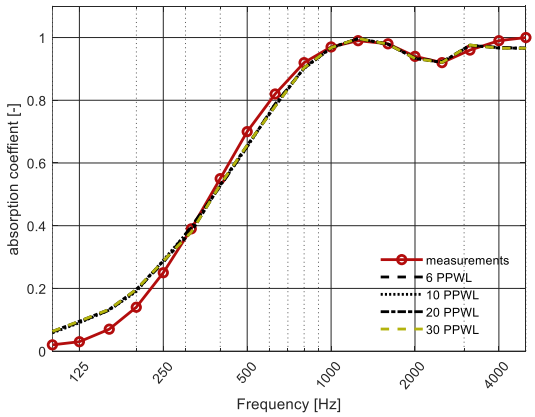

Figure 8. Measured normal incidence sound absorption compared to 1D FDTD simulations using different PPWL values for a 60 mm melamine sheet.

3.3.2 Minimum simulation time

As previously discussed, the 2D FDTD calculation requires a sinusoidal input signal due to the presence of periodic boundaries. A key challenge with this configuration is the time required for the signal to fully propagate at high incidence angles. This issue is illustrated in Figure 9, which presents space-time plots. Before the signal stabilizes, a ripple effect can be observed in the plots.

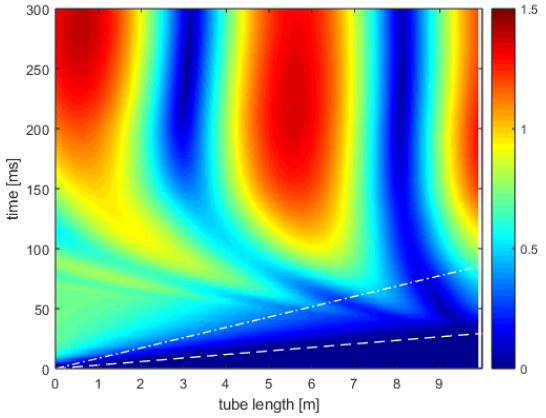

Figure 9. Space-time plot for a 60 mm melamine sheet at 100 Hz and 70º incidence angle. Absolute pressure values are represented with [0-300] ms time. White continuous line represent the first NEAM layer, dashed line c_0, and dotted-dash $c_0 \cdot \cos(\theta)$.

In most cases, the absorption coefficient reaches an accurate value after a simulation time of less than 50 ms for low incidence angles. However, at higher angles, the ripple effect becomes more pronounced. Extending the propagation time helps stabilize the pressure, allowing convergence to the final absorption coefficient within a defined tolerance.

To aid in the analysis, the received signal can be averaged over the final milliseconds of each simulation. This approach eliminates the initial period before the signal reaches the NEAM interface and minimizes the impact of potential spatial pressure variations. A mean squared error (MSE) analysis was performed to assess the variation in absorption coefficient estimation over time, showing a progressive reduction in error and convergence toward the measured value.

For higher incidence angles, the MSE curves exhibit more oscillations, indicating a less uniform convergence process, though convergence is still achieved. To better evaluate a possible convergence criterion while mitigating the effect of these oscillations, a smoothed MSE curve was also computed (represented by green lines in the figure 10). Using this approach, even in the most challenging scenario (1 kHz at 80º), a clear convergence criterion can be established, allowing for a systematic selection of the stopping point in the simulation process.

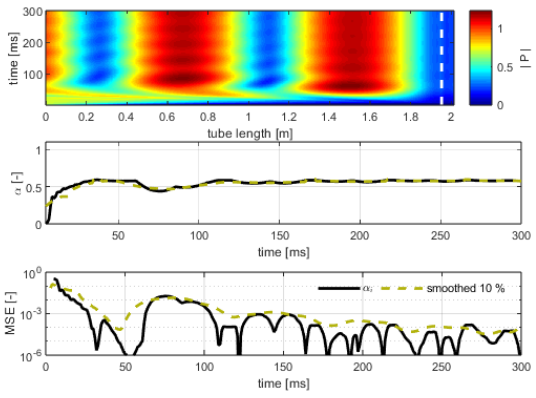

Figure 10. Computation for a 60 mm melamine sheet for 1 kHz at 80º, divided in three rows: 1) Absolute space-time pressure, 2) Diffuse absorption coefficient calculated using different true values, 3) Mean Squared Error (MSE) with the black line representing the error using the last time pressure to calculate the true value of the absorption coefficient, and dotted green line a 10 % sample smooth with an average of the last 150 ms as the true value.

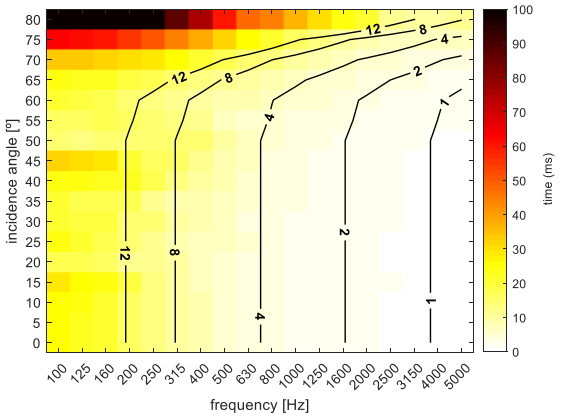

Figure 11. Minimum propagation time needed to compute the diffuse field sound absorption coefficient of a 60 mm melamine sheet, for each angle and frequency, with an error of 10-3. True value of alpha was calculated with an average of the last 150 ms calculation.

Figure 11 illustrates the propagation time required for a complete simulation using an MSE of 10^{-3} as the stopping criterion. In this color plot, white and black shades represent shorter and longer simulation times, respectively. It is evident that, with the exception of very high incidence angles and low frequencies, simulation times under 50 ms are adequate to achieve the desired tolerance.

3.3.3 Computational costs

A key factor in the algorithm's performance is the time required to complete a full material study using 2D FDTD with 20 PPWL across the entire frequency range, considering all angles. For frequencies between 315 Hz and 5 kHz, the total computational time was 15 hours. However, below 315 Hz and for high incidence angles, the computation time increases significantly, with 212 hours needed just for the 100 Hz to 315 Hz range. This is due to the larger simulation space required for high angles and low frequencies, resulting in very high computational costs.

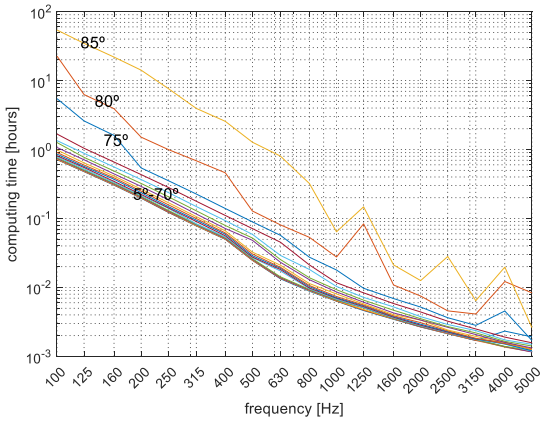

Figure 12. Real time expended computing on 2D FDTD melamine foam simulation for incidence angles in the range [5º-85º] with 5º step and 20 PPWL.

4. CONCLUSIONS

As demonstrated throughout this document, a fluid-like linear propagation model for absorbent materials has been developed, which can be adapted to common types of media such as porous materials and fibers. The model exhibits strong correlation between laboratory measurements and results obtained via the FDTD method. It has been shown that with a single measurement of the absorption coefficient at normal incidence, the model can accurately characterize the material's frequency response, the surface impedance and diffuse absorption coefficient. The 2D-FDTD method also aligns well with analytical data for infinite samples, though it remains uncertain whether the 1D-FDTD coefficient values can be applied to 3D simulations. Additionally, it has been confirmed that computational time can be optimized by reducing the PPWL number without negatively impacting absorption coefficient characterization. However, reducing the PPWL ratio leads to a loss of certain physical details about the material. Nonetheless, due to a lack of information, the reliability of the method at frequencies below 315 Hz cannot be guaranteed, with a slight overestimation of the absorption coefficient expected at lower frequencies.

5. ACKNOWLEDGMENTS

This work was supported by the Spanish Ministry of Economy and Innovation (MINECO) and the European Union FEDER (project PID2019-109175GB-C22). This work was partly financed by FCT / MCTES through national funds PIDDAC under the R&D ISISE, under reference UID / 04029/2020, and under ARISE reference LA/P/0112/2020.

6. REFERENCES

[1] Keith ATTENBOROUGH, "Acoustical characteristics of porous materials," Physics reports, vol. 82, no. 3, pp. 179-227, 1982.

[2] Z. E. A. FELLAH, et al, "Transient acoustic wave propagation in rigid porous media: A time-domain approach," The Journal of the Acoustical Society of America, vol. 107, no. 2, pp. 683-688, 2000.

[3] M. FELLAH, et al, "Generalized hyperbolic fractional equation for transient-wave propagation in layered rigid-frame porous materials," Physical Review E, vol. 77, no. 1, p. 016601, 2008.

[4] Denis LAFARGE, et al, "Dynamic compressibility of air in porous structures at audible frequencies," The Journal of the Acoustical Society of America, vol. 102, no. 4, pp. 1995-2006, 1997.

[5] Antoni ALOMAR, et al, "Time-domain simulation of a flow duct with extended-reacting acoustic liners," eForum Acusticum, pp. 407-409, 2020.

[6] Ilyes MOUFID, et al, "Energy analysis and discretization of the time-domain equivalent fluid model for wave propagation in rigid porous media," Journal of Computational Physics, vol. 451, p. 110888, 2022

[7] Heinrich KUTTRUFF, Acoustics: an introduction.: CRC Press, 2007.

[8] Allen TAFLOVE,et al, Computational Electrodynamics: The Finite-Difference Time-Domain Method 3rd edn.: Norwood, MA: Artech House, 2005.

[9] Trevor J. COX and Peter D'ANTONIO, Acoustic absorbers and diffusers: theory, design and application.: CRC Press, 2009.

[10] Matheus PEREIRA, et al, "Proposal of numerical models to predict the diffuse field sound absorption of finite sized porous materials–BEM and FEM approaches," Applied Acoustics, vol. 180, no. 108092, 2021.

[11] Romina del REY TORMOS, et al, "Nuevos materiales absorbentes acústicos obtenidos a partir de restos de botellas de plástico," 2011.